FOUNDATIONS ADVANCES

ISSN 2053-2733

# Enhanced X-ray structural analysis using total variation denoising of X-ray diffraction images

Kouhei Ichiyanagi,[a]* Toshiyuki Sasaki,[a] Yuichi Yokoyama[a]* and Yuichi Yamasaki[b,c]

[a]Japan Synchrotron Radiation Research Institute, 1-1-1 Kouto, Sayo, Hyôgo 679-5198, Japan, [b]National Institute for Materials Science, 1-2-1 Sengen, Tsukuba, Ibaraki 305-0047, Japan, and [c]International Center for Synchrotron Radiation Innovation Smart (SRIS), Tohoku University, 468-1 Aramaki Aza Aoba, Sendai, Miyagi 980-8572, Japan. *Correspondence e-mail: kichiyanagi@spring8.or.jp, y.yokoyama@spring8.or.jp

Received 6 June 2025
Accepted 31 October 2025

Edited by B. J. Campbell, Brigham Young University, USA

**Keywords:** X-ray structure analysis; denoising method; total variation regularization.

**Supporting information:** this article has supporting information at journals.iucr.org/a

A denoising method based on total variation regularization was applied to X-ray diffraction images obtained from X-ray crystallography experiments. This approach significantly enhanced the signal-to-noise ratio of weak diffraction spots. Subsequently, the denoised images were used for crystal structure data processing using cytidine as a standard sample, which yielded an improved structural analysis result. This image processing technique offers a practical method for improving the quality of weak diffraction data, which is particularly relevant for challenging samples such as microcrystals, thereby enabling more reliable crystallographic analysis.

## 1. Introduction

Accurate determination of crystal and molecular structure via X-ray crystallography is crucial and relies on diffraction data encompassing high-order reflections from the sample crystal. Advances in intense X-ray sources and highly sensitive area detectors have facilitated the measurement of the weak reflections associated with these high-order reflections. However, the contemporary trend towards crystal minimization (Takaba *et al.*, 2023; Schriber *et al.*, 2022), coupled with X-ray irradiation-induced data degradation from crystal damage, presents formidable challenges to achieving high-resolution data. Notably, high-order X-ray diffraction reflections, which are important for high-resolution information, often exhibit intensities that are two to three orders of magnitude lower than those of fundamental reflections, further hindering their detection. Consequently, a substantial number of high-order X-ray diffraction spots remain obscured by noise, leading to incomplete dataset analysis with insufficient completeness for X-ray structural studies.

This issue is particularly pronounced in X-ray crystallography of unstable single crystals, where samples are highly susceptible to radiation damage, and in the analysis of microcrystals. Diffraction spots from high-order reflections are paramount in precision X-ray structure analysis, with the completeness of high-order reflection data being a key determinant (Hara *et al.*, 2024; Kitou *et al.*, 2017; Kitou *et al.*, 2020). So far, noise reduction methods for 1D X-ray diffraction data and X-ray diffraction tomography have been validated by filtering methods (Le *et al.*, 2023; Chukhovskii *et al.*, 2022). Also, a noise reduction method for X-ray single-particle images using a neural network has been reported (Bellisario *et al.*, 2022). The application of various noise reduction methods is not confined to X-ray pulse imaging and X-ray tomography but also extends to X-ray structural analysis, both of which

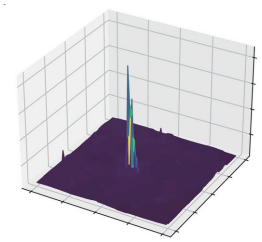

**Table 1**
Summary of SCXRD experimental conditions and crystallographic data obtained from analysis of the raw dataset of cytidine.

| | |
|---|---|
| Wavelength (Å) | 0.8124 |
| Temperature (K) | 100 |
| Measurement $\omega$ angle (°) | −90 to 90 |
| Step angle $\Delta\omega$ (°) per image | 1 |
| $\varphi$ angle (°) | 0, 90, 270, 360 |
| $\kappa$ angle (°) | 45 |
| Exposure time (s) per image | 0.25 |
| $D$ (mm), camera distance | 52.11 |
| $2\theta$ angle of detector (°) | 25 |

necessitate the detection of weak signals. On the other hand, X-ray diffraction imaging using denoising techniques based on sparse modeling has already been reported (Yokoyama *et al.*, 2019; Yokoyama *et al.*, 2022). Given the inherent difficulty in enhancing the signal-to-noise ratio in weak diffraction spots of X-ray measurements, the development and implementation of robust denoising methodologies will be pivotal for future X-ray measurements and their data analysis.

Sparse modeling offers a robust approach to data analysis in the presence of noise and incomplete information by utilizing prior knowledge about the sample (Yokoyama *et al.*, 2019; Yokoyama *et al.*, 2022). Among its analytical methods, total variation (TV) regularization is employed as a denoising technique to distinguish noise components, which exhibit pixel-wise uncorrelated behavior, from the observed image. TV regularization is a widely adopted technique for noise reduction. Compared with alternative methods, such as Gaussian filtering, TV denoising offers the distinct advantage of effectively preserving edges while simultaneously mitigating background noise in uniform regions. Conventional crystal structure analysis determines crystal and molecular structure by precisely measuring the integrated intensities of a large number of observed diffraction spots, which are then used to build and refine a structural model. Therefore, it is crucial to collect as many independent diffraction spots as possible for improved analytical accuracy. To analyze complex diffraction image data, TV denoising is a particularly effective approach because it can improve statistical accuracy without requiring large-scale training data. Therefore, TV denoising is well suited for situations where diffraction patterns change due to variations in sample symmetry or measurement conditions.

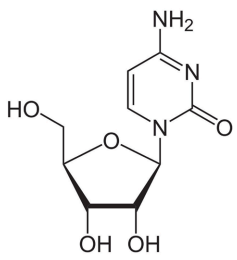


**Figure 1**
Chemical structure of cytidine.

To assess the efficacy of this denoising approach in X-ray crystallography, we applied TV denoising to 2D X-ray diffraction images. Our analysis focuses on evaluating how this method for enhancing molecular structure determination can be implemented.

## 2. Dataset of X-ray diffraction images for structural analysis

To evaluate the efficacy of TV denoising of X-ray crystallography image data, a dataset for structural analysis was acquired at the SPring-8 BL40XU EH2 beamline (Yasuda *et al.*, 2009; Yasuda *et al.*, 2010; Yasuda & Kimura, 2019). A helical undulator was installed in the BL40XU beamline. A Si(111) channel-cut monochromator was used to monochromatize the X-rays from a narrow X-ray energy bandwidth ($\Delta E/E \simeq 2\%$). The X-ray beam size was 150 × 150 µm at the sample position. The photon flux of the monochromatic X-ray beam was approximately $10^{10}$ photons $s^{-1}$. Cytidine ($C_9H_{13}N_3O_5$), illustrated in Fig. 1, was used as a demonstration sample for the TV denoising process. The single crystal of cytidine was cut into an approximately 0.05 mm cube for structure analysis from X-ray diffraction images. The experimental parameters and crystal data of raw datasets are summarized in Table 1. The diffraction images were collected using an EIGER 1M (DECTRIS Ltd) detector. A comprehensive description of the X-ray diffraction measurement system is provided by Yasuda & Kimura (2019). To ensure high completeness for the X-ray structure analysis, the crystal was fixed at $\chi = 45°$, and diffraction data were collected by performing $\omega$ scans at different $\phi$ angles. The $\phi$ angle was rotated 0°, 90°, 180°, 270°, and the $\omega$ axis was rotated −90 to 90° at each $\phi$ axis angle to acquire the dataset. The results of the crystallographic analysis of cytidine are presented in Table S1 (in the supporting information).

## 3. Structural analysis with the TV denoising process

### 3.1. X-ray diffraction images with TV denoising

TV regularization is a technique used in image processing and other fields to reduce random noise while preserving sharp edges. It is based on the principle that images tend to have correlation between neighboring pixels. TV regularization exploits this property to distinguish between noise and genuine image features.

The TV denoised image $\mathbf{y}$ is obtained as

$$\mathbf{y} = \arg\min_{\mathbf{y}} \left( \frac{1}{2} \|\mathbf{x} - \mathbf{y}\|_{l_2}^2 + \alpha \|\nabla \mathbf{y}\|_{\mathrm{TV}}^1 \right), \tag{1}$$

where $\mathbf{x}$ corresponds to the observed X-ray diffraction image. $\|\cdot\|_{l_2}$ denotes the $\ell_2$ norm, while $\|\cdot\|_{\mathrm{TV}}$ is the TV norm defined by

$$\|\nabla \mathbf{y}\|_{\mathrm{TV}}^1 = \sum_{i,j} \sqrt{\left(y_{i+1,j} - y_{i,j}\right)^2 + \left(y_{i,j+1} - y_{i,j}\right)^2}.$$

$\alpha$ represents the regularization parameter which controls the amount of noise reduction. Equation (1) is solved by the primal–dual splitting method which does not require calculation of the inverse matrices that are computationally expensive to calculate (Chambolle, 2004; Yokoyama *et al.*, 2022). In this method, by using the dual variable $\mathbf{p} = (\mathbf{p}^1, \mathbf{p}^2)$, the update equation for the $k$th iteration is expressed as

$$\left(\mathbf{p}_{k+1}\right)_{i,j} = \frac{\left(\mathbf{p}_k\right)_{i,j} + \tau\left[\nabla(\nabla \cdot \mathbf{p}_k) - \mathbf{x}/\alpha\right]_{i,j}}{1 + \tau\left|\nabla(\nabla \cdot \mathbf{p}_k) - \mathbf{x}/\alpha\right|}. \tag{2}$$

Here $\tau$ is a hyperparameter for the dual variable. The value of $\tau$ was set to 1/8 because the convergence of equation (2) has been proven in the range of $\tau \leq 1/8$ (Chambolle, 2004). The primal–dual splitting method starts from the initial value $\mathbf{p}_0 = (\mathbf{0}, \mathbf{0})$, where $\mathbf{0}$ denotes zero matrix. After a sufficient number of iterations have led to convergence, the TV denoised image is obtained as $\mathbf{y} = \mathbf{x} - \alpha\nabla \cdot \mathbf{p}_k$. Our algorithm was implemented from scratch in Python. TV denoising of one image is completed in 20 s for a 1065 × 1065 pixel image on a workstation equipped with a CPU (Intel Core i9-9980XE CPU @ 3.00 GHz).

Fig. 2(*a*) shows the denoising results of one X-ray diffraction image with regularization parameters $\alpha$ = 0.5, 1.0, 2.0. Figs. 2(*b*) and 2(*c*) then demonstrate the effect of the increasing parameter value, showing 3D surface plots of the (−14 −10 −1) and (10 −15 1) diffraction spots, with the enhanced clarity.

This method effectively reduces background noise originating from the detector and the instrument function. The

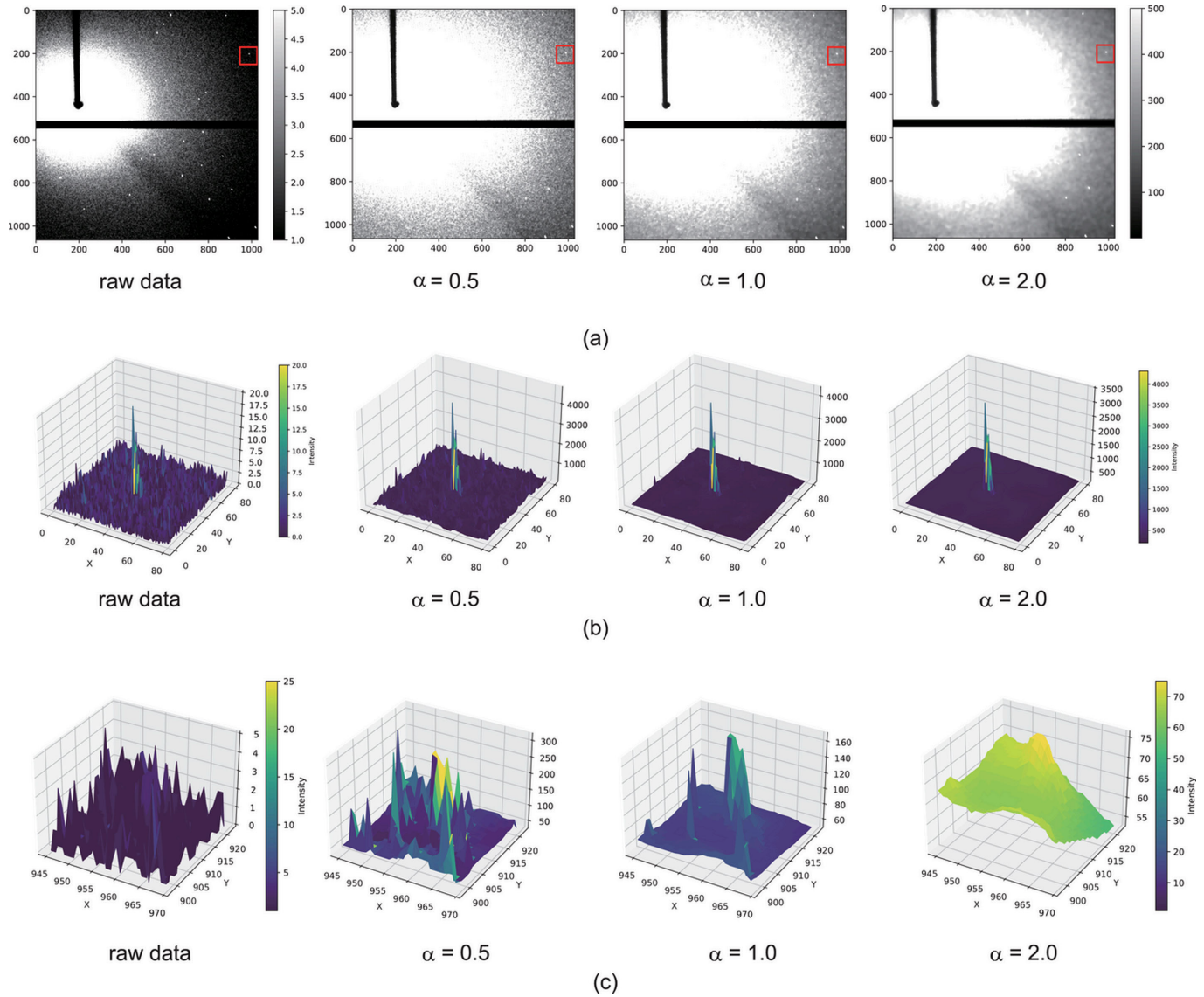


**Figure 2**
(*a*) A typical raw X-ray diffraction image and its corresponding TV denoising images obtained using various values of the regularization parameter are shown. (*b*) 3D surface plots of intensity for the region highlighted by a red square [indicating the (−14 −10 −1) reflection] from each corresponding image shown in (*a*). Pixel values were normalized for data processing following the TV denoising process. (*c*) 3D surface plots of intensity for the (10 −15 1) reflection, obtained from a different raw image and its corresponding TV denoising images.

**Table 2**
Summary of datasets processed with different denoising parameters, showing $R_1$, $wR_2$, $R_{int}$ values after refinement, and the number of unique reflections.

The $R$ factor, $R_1$, is a residual index that quantifies the agreement between the observed ($F_o$) and the calculated ($F_c$) structure factor derived from the structural model. $wR_2$ is the weighted $R$ factor, a goodness-of-fit indicator based on the squared structure factor ($F_o^2$).

| $\alpha$ | $R_1$ (%) | $wR_2$ (%) | $R_{int}$ (%) | No. of unique reflections |
|---|---|---|---|---|
| 0 (Raw data) ($d_{min}$ = 0.76 Å) | 6.87 | 18.39 | 16.4 | 2326 |
| 0.5 ($d_{min}$ = 0.74 Å) | 5.73 | 15.01 | 17.07 | 2451 |
| 1.0 ($d_{min}$ = 0.74 Å) | 5.62 | 14.53 | 17.2 | 2450 |
| 2.0 ($d_{min}$ = 0.74 Å) | 6.05 | 15.28 | 17.55 | 2451 |

core principle is to remove background noise, which is characterized by a lack of pixel-to-pixel correlation. Consequently, signals that possess inherent pixel-to-pixel correlation, such as diffraction spots, air scattering, diffuse scattering and other scattering from instruments, are preserved, enabling reflections previously buried in noise to be recovered as valid, processable data after TV denoising.

As the regularization parameter $\alpha$ increases, the denoising effect is enhanced and the background becomes progressively flatter. When applied appropriately, our denoising process reduces the integrated intensity error associated with high-order *hkl* reflections, enabling the identification and extraction of signals that were previously obscured by background noise.

### 3.2. Structure analysis from denoised X-ray diffraction images

For the comparative analysis between the raw and denoised datasets, structure determination was performed using a standard workflow for single-crystal X-ray diffraction (SCXRD). First, the data were processed using *XDS* [*X-ray Detector Software* (Kabsch, 2010)] to generate an *hkl* file from each X-ray diffraction image dataset. Subsequently, structure solution and least-squares refinement were performed using *SHELXT* and *SHELXL*, respectively (Sheldrick, 2015*a*; Sheldrick, 2015*b*) within the *Olex2* program suite (Dolomanov *et al.*, 2009).

In conventional X-ray structure analysis, *hkl* data processing is applied directly to the raw image dataset. In this study, a TV denoising process was implemented prior to this standard image processing. Following noise reduction of all X-ray diffraction images, structure analysis proceeded using the established workflow. After TV denoising, the data were converted from float to integer type and then normalized. The structure determination results obtained from the denoised data were then compared with those derived from the raw image dataset. A total of 720 images in the dataset were denoised using various regularization parameters. After the indexing process, four datasets were merged.

Application of TV denoising increased the number of high-angle diffraction spots, leading to an improved resolution. This indicates that the diffraction data were successfully measured to the outermost edge of the detector. Detailed results of the data processing with *XDS* for both the raw and denoised datasets are shown in Tables S2, S3 and S4 of the supporting information.

Fig. 3 shows the results of the structural analysis under each TV denoising condition in terms of $I/\sigma I$ and $R_{int}$, the evaluation parameters for refinement in structural analysis. Fig. 3(*a*) compares the $I/\sigma I$ as a function of $d$ spacing extracted from images processed with various regularization parameters. The $I/\sigma I$, which is a measure of the signal-to-noise ratio, generally decreases with increasing resolution. Although the highest-resolution data in the raw images were buried in background noise, all diffraction spots in the denoised X-ray diffraction images were successfully extracted with a significance level of at least 3$\sigma$. Fig. 3(*b*) shows that $R_{int}$ factors depend on the $d$ spacing, indicating the deviation among symmetry-equivalent reflections with various regularization parameters. A low $R_{int}$ value signifies high precision in the measured data. This value

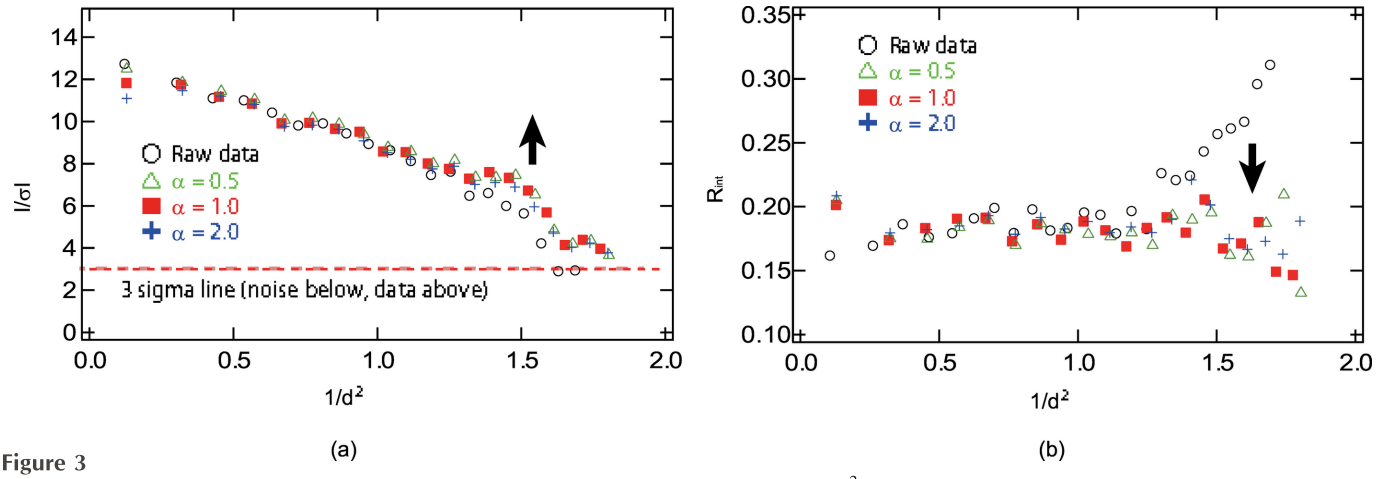


**Figure 3**
Refinement results for cytidine using *SHELXL* for raw and denoised data as a function of $1/d^2$. (*a*) $I/\sigma I$ values obtained after refinement for the raw data and for data denoised with $\alpha$ = 0.5, 1.0 and 2.0. The red dotted line indicates the 3$\sigma$ criterion. (*b*) Corresponding $R_{int}$ factors as a function of $1/d^2$. The internal $R$ factor, $R_{int}$, is a data quality value that measures the internal consistency of the dataset. It quantifies the agreement among symmetry-equivalent reflections.

typically increases with decreasing $d$ spacing and this trend was observed in the raw data. This indicates that the variance in the high-angle data, corresponding to high-order $hkl$ reflections, was effectively reduced. These $R_{\rm int}$ values improved significantly after TV denoising, especially for high-resolution diffraction spots, and showed a trend similar to that of low-resolution reflections.

## 4. Comparison of structure analysis results using each denoised dataset

Table 2 presents the results of X-ray structure analysis using $hkl$ data derived from both the TV denoised and raw image datasets. All structural analyses yielded consistent unit-cell, symmetry and crystallographic parameters. Structural analysis could be performed without problems using the denoised dataset. After TV denoising of X-ray diffraction images, the number of unique diffraction peaks clearly increased, and the minimum resolution also decreased from 0.76 to 0.74 Å. Moreover, the $R_1$ and $wR_2$ values showed a reduction after TV denoising. This improvement is attributed to the significant enhancement in the quality of weak diffraction spots in the high-angle diffracted area. The TV denoising process enables the achievement of the maximum resolution potential of the detector under the current measurement conditions without increasing the exposure time. This demonstrates the effectiveness of the TV denoising process for 2D diffraction images in X-ray structural analysis.

In the denoising process of TV regularization the amount of denoising applied can be controlled by adjusting the parameter $\alpha$, but it is difficult to derive the optimal value. When comparing the results of the structure analysis for an $\alpha$ value between 1.0 and 2.0, the $R$ values slightly increased despite the higher noise reduction effect. In fact, as $\alpha$ is increased, the noise reduction can also lead to a decrease in the intensity of strong diffraction spots, and the linearity of integrated diffraction spots can be compromised. To maximize the effectiveness of the noise reduction using TV regularization, we propose investigating alternative noise reduction strategies or adjustments to the current approach that could preserve the integrity of strong diffraction peaks while still effectively reducing noise. While optimization of the regularization parameter, $\alpha$, is necessary, our results demonstrate that the denoising method using TV regularization can enhance the accuracy of X-ray structural analysis.

Our method has a very low computational cost for denoising a single image. The resulting improvement in the signal-to-noise ratio of the diffraction spots in the datasets clearly enhances the final results of the structural refinement. Nevertheless, the inherent quality of the crystal remains a primary limiting factor. Therefore, it is unlikely that this method alone can solve a crystal structure that is unsolvable due to fundamentally poor crystallinity. We tested the method on datasets with poor diffraction quality, previously deemed unpublishable. While the noise reduction technique provided some improvement, it was insufficient to render the data publishable at this stage. Future development will be aimed at enhancing the algorithm's ability to reliably identify and extract weak peaks obscured by noise within poor-quality datasets.

This noise reduction technique is expected to be particularly useful for X-ray diffraction images, especially for diffraction data with weak intensity, such as those obtained from microcrystals whose structures are often challenging to determine. Having established the effectiveness of this noise reduction technique in this paper, future work will focus on developing a model-based approach to optimize the regularization parameter, $\alpha$, which was heuristically selected in this study for X-ray structural analysis.

## 5. Summary

In this study, we applied a denoising method based on TV regularization, a sparse modeling technique, to 2D X-ray diffraction image data obtained from single-crystal X-ray crystallography experiments. We compared the results of X-ray structural analysis using both the denoised and raw image datasets of cytidine. Our findings demonstrate that TV denoising effectively enhances the signal-to-noise ratio of weak X-ray diffraction spots. This improvement was evident in the enhanced quality of the final structure refinement.

The applicability of this denoising approach extends to a wide range of challenging single-crystal structure analyses where diffraction intensities are inherently weak. Our technique could be a valuable tool for extracting reliable structural information from such diffraction image datasets. However, a direct validation on a broader range of crystals was beyond the scope of this initial report. Nevertheless, we believe the practical verification of this method across diverse fields of single-crystal analysis is a compelling avenue for future research.

## Acknowledgements

The synchrotron radiation experiments were performed on beamline BL40XU EH2 at SPring-8 with the approval of the Japan Synchrotron Radiation Research Institute (JASRI) (proposal Nos. 2022B2115, 2023A2337, 2023B2428, 2023B1422 and 2024A1782). We thank Professors Masato Okada and Masaichiro Mizumaki for supporting this study.

## Conflict of interest

No conflict of interest is declared.

## Data availability

The Python code for TV denoising and the datasets used during the current study are available from the corresponding author on reasonable request.

## Funding information

This work was partially supported by JST, CREST under grant Nos. JPMJCR1861 and JPMJCR2435, JSPS KAKENHI under grant Nos. JP22K05054 and JP21H01677, and JST PRESTO under grant No. JPMJPR25JA.

## References

Bellisario, A., Maia, F. R. N. C. & Ekeberg, T. (2022). *J. Appl. Cryst.* **55**, 122–132.

Chambolle, A. (2004). *J. Math. Imaging Vis.* **20**, 89–97.

Chukhovskii, F. N., Konarev, P. V. & Volkov, V. V. (2022). *J. Mater. Sci. Appl.* **6**, 1–12.

Dolomanov, O. V., Bourhis, L. J., Gildea, R. J., Howard, J. A. K. & Puschmann, H. (2009). *J. Appl. Cryst.* **42**, 339–341.

Hara, T., Hasebe, M., Tsuneda, T., Naito, T., Nakamura, Y., Katayama, N., Taketsugu, T. & Sawa, H. (2024). *J. Am. Chem. Soc.* **146**, 23825–23830.

Kabsch, W. (2010). *Acta Cryst.* D**66**, 125–132.

Kitou, S., Fujii, T., Kawamoto, T., Katayama, N., Maki, S., Nishibori, E., Sugimoto, K., Takata, M., Nakamura, T. & Sawa, H. (2017). *Phys. Rev. Lett.* **119**, 065701.

Kitou, S., Hosogi, Y., Kitaura, R., Naito, T., Nakamura, T. & Sawa, H. (2020). *Crystals* **10**, 998.

Le, D. P., Deijkers, J. A., Kim, Y. D., Wadley, H. N. G. & Aspnes, D. E. (2023). *J. Vac. Sci. Technol. B* **41**, 044004.

Schriber, J., Paley, D. W., Bolotovsky, R., Rosenberg, D. J., Sierra, R. G., Aquila, A., Mendez, D., Poitevin, F., Blaschke, J. P., Bhowmick, A., Kelly, R. P., Hunter, M., Hayes, B., Popple, D. C., Yeung, M., Pareja-Rivera, C., Lisova, S., Tono, K., Sugahara, M., Owada, S., Kuykendall, T., Yao, K., Schuck, P. J., Solis-Ibarra, D., Sauter, N. K., Brewster, A. S. & Hohman, J. N. (2022). *Nature* **601**, 360–365.

Sheldrick, G. M. (2015*a*). *Acta Cryst.* A**71**, 3–8.

Sheldrick, G. M. (2015*b*). *Acta Cryst.* C**71**, 3–8.

Takaba, K., Maki-Yonekura, S., Inoue, I., Tono, K., Hamaguchi, T., Kawakami, K., Naitow, H., Ishikawa, T., Yabashi, M. & Yonekura, K. (2023). *Nat. Chem.* **15**, 491–497.

Yasuda, N., Fukuyama, Y., Toriumi, K., Kimura, S., Takata, M., Garrett, R., Gentle, I., Nugent, K. & Wilkins, S. (2010). *AIP Conf. Proc.* pp. 147–150.

Yasuda, N. & Kimura, S. (2019). *AIP Conf. Proc.* **2054**, 050007.

Yasuda, N., Murayama, H., Fukuyama, Y., Kim, J. E., Kimura, S., Toriumi, K., Tanaka, Y., Moritomo, Y., Kuroiwa, Y., Kato, K., Tanaka, H. & Takata, M. (2009). *J. Synchrotron Rad.* **16**, 352–357.

Yokoyama, Y., Arima, T., Okada, M. & Yamasaki, Y. (2019). *J. Phys. Soc. Jpn* **88**, 024009.

Yokoyama, Y., Yamasaki, Y., Okada, M. & Mizumaki, M. (2022). *J. Phys. Soc. Jpn* **91**, 034701.